




# Largely enhanced luminescence intensity and improved optical temperature sensing properties in $\text{CaWO}_4\text{-La}_2(\text{WO}_4)_3$ : $\text{Er}^{3+}$ , $\text{Yb}^{3+}$ via regulating cations composition

Ying Zhang<sup>1,2,3</sup> , Xusheng Wang<sup>3,\*</sup>, Qian Liu<sup>1,\*</sup>, and Zhitang Song<sup>2</sup>

<sup>1</sup> State Key Laboratory of High Performance Ceramics and Superfine Microstructure, Shanghai Institute of Ceramics, Chinese Academy of Sciences, Shanghai 200050, China

<sup>2</sup> State Key Laboratory of Functional Materials for Informatics, Shanghai Institute of Microsystem and Information Technology, Chinese Academy of Sciences, Shanghai 200050, China

<sup>3</sup> Functional Materials Research Laboratory, School of Materials Science and Engineering, Tongji University, Shanghai 201804, China

Received: 3 June 2020

Accepted: 4 September 2020

Published online:

15 September 2020

© Springer Science+Business Media, LLC, part of Springer Nature 2020

## ABSTRACT

High temperature sensing sensitivity and luminescence intensity of phosphors are crucial factors for excellent optical temperature sensing performance. Based on material design, the pure phase and two-phase solid solutions were prepared by regulating the relative content of cations  $\text{Ca}^{2+}$  and  $\text{La}^{3+}$  in  $\text{CaWO}_4\text{-La}_2(\text{WO}_4)_3$ , respectively. The up-conversion luminescence (UCL) and optical temperature sensing performance of rare earth ions  $\text{Er}^{3+}/\text{Yb}^{3+}$  co-doped  $\text{CaWO}_4\text{-La}_2(\text{WO}_4)_3$  were studied. As guided by regulating cation composition through partial substituting  $\text{Ca}^{2+}$  ions by  $\text{La}^{3+}$  ions, the UCL intensity of two-phase solid solutions at 552 nm is much higher than that of pure phase material. The UCL intensity of  $0.2\text{La}_2(\text{WO}_4)_3\text{-}0.8\text{CaWO}_4$ : 1% $\text{Er}^{3+}$ , 5% $\text{Yb}^{3+}$  is as 33.5 times as that of  $\text{CaWO}_4$ : 1% $\text{Er}^{3+}$ , 5% $\text{Yb}^{3+}$  material. More importantly, the high temperature sensing sensitivity ( $0.01026\text{ K}^{-1}$ ) is achieved in a wider temperature range 83–683 K in optimal UCL material  $0.2\text{La}_2(\text{WO}_4)_3\text{-}0.8\text{CaWO}_4$ : 1% $\text{Er}^{3+}$ , 5% $\text{Yb}^{3+}$ . It is suggested that material design theory can be used as a powerful tool to accelerate discovery of novel optical temperature sensing materials, with implications even for the design of other optoelectronic materials.

Address correspondence to E-mail: xs-wang@tongji.edu.cn; qianliu@mail.sic.ac.cn

## 1 Introduction

Since the New Year of 2020, novel coronavirus has spread worldwide [1]. Fever is one of the important criteria for the diagnosis of coronavirus disease 2019 (COVID-19) [2]. Non-contact laser infrared thermometer can quickly and accurately measure human body temperature (32.0–42.5 °C) without contact [3], and it plays a very important role in the fight against epidemic diseases. However, in the field of scientific research and industrial production, there are some harsh environments, such as power stations, oil refineries, and coal mines. [4–7] And non-contact optical pyrometer, total-radiation pyrometer, and infrared thermometer are easily affected by external factors, such as emissivity, measurement distance, dust, and water vapor of the measured object, which often lead to large measurement errors. Therefore, it is crucial to research and develop high-precision non-contact temperature sensors [8–10].

The fluorescence intensity ratio (FIR) technique is less dependent on measuring conditions, not limited by the fluorescence loss, the fluctuation of the intensity of the excitation light source, and the number and distribution of the luminescent centers [11–13]. Therefore, it is considered as a more potential application of temperature measurement technology, which has attracted great attention from researchers. In addition, some rare earth ions, such as  $\text{Pr}^{3+}$  [14],  $\text{Ho}^{3+}$  [15],  $\text{Nd}^{3+}$  [16],  $\text{Tm}^{3+}$  [17], and  $\text{Er}^{3+}$  [7, 18], possess not only rich energy levels, but also thermally coupled energy level pairs. Therefore, the emissions generated by the rare earth ion-doped fluorescence materials can be used to measure temperature by FIR technique.

Compared with many other optical temperature sensing materials, tungstates have excellent optical temperature sensing property and has been widely studied. Among them, the UCL intensity of multiphase strontium tungstate is far higher than that of pure  $\text{SrWO}_4$ , and its optical temperature sensing performance is excellent [19]. In addition, for  $\text{KY}(\text{WO}_4)_2\text{-K}_2\text{WO}_4$  materials, the UCL performance of the multiphase material is optimal, and the sensitivity  $S$  is very high in a very wide temperature range (83–663 K). The maximum sensitivity reaches  $0.0147 \text{ K}^{-1}$  at 643 K [20]. The results above brought us an inspiration that one or two tungstate materials with stable chemical properties and excellent optical temperature sensing property can be selected and

designed as multiphase tungstate materials or two-phase solid solution materials. It is hoped that by means of material design, composition and microstructure of the material will change, and thus improve the performance of the materials. In other words, in a sufficiently wide temperature range, with the increase of temperature, the UCL intensity and temperature sensing sensitivity  $S$  can both maintain sufficiently high values, which are the goal of optical temperature sensors in the future practical applications.

Due to the ion radius and chemical properties of rare earth ion  $\text{La}^{3+}$  similar to activator and sensitizer, most of its inorganic compounds are suitable UCL hosts. Besides, the rare earth ion-doped [11, 21–23] materials are widely studied for its bright UCL and excellent optical temperature sensing performance. Therefore,  $\text{CaWO}_4$  and  $\text{La}_2(\text{WO}_4)_3$  were selected as research objects in this study. Based on material design, a series of UCL materials with pure phase and two-phase solid solutions as hosts were synthesized by regulating the composition of cations  $\text{Ca}^{2+}$  and  $\text{La}^{3+}$ . In the study of rare earth ions  $\text{Er}^{3+}/\text{Yb}^{3+}$  co-doped  $\text{CaWO}_4\text{-La}_2(\text{WO}_4)_3$  phosphors, the UCL intensity of two-phase solid solutions is much higher than those of pure  $\text{CaWO}_4$  and  $\text{La}_2(\text{WO}_4)_3$ . Moreover, the two-phase solid solution tungstate materials could maintain high temperature sensing performance in a wide temperature range.

## 2 Experiments

Rare earth ions  $\text{Er}^{3+}/\text{Yb}^{3+}$  co-doped  $\text{CaWO}_4\text{-La}_2(\text{WO}_4)_3$  phosphors were designed as  $x\text{La}_2(\text{WO}_4)_3\text{-(1-x)CaWO}_4$  ( $x = 0, 0.2, 0.4, 0.6, 0.8, 1$ ) and synthesized by the solid-state reaction method. In order to study the effects of different hosts on UCL performance, the concentrations of rare earth ions  $\text{Er}^{3+}$  and  $\text{Yb}^{3+}$  were fixed at 1 mol% and 5 mol%, respectively. A series of UCL materials were synthesized by regulating the composition of cations  $\text{Ca}^{2+}$  and  $\text{La}^{3+}$ . The specific preparation process is as follows: Stoichiometric amounts of raw materials  $\text{CaCO}_3$  (99.9%, Sinopharm Chemical Reagent Co. Ltd.),  $\text{WO}_3$  (99.8%, Alfa Aesar),  $\text{La}_2\text{O}_3$  (99.99%, Sinopharm Chemical Reagent Co. Ltd.),  $\text{Er}_2\text{O}_3$  (99.9%, Sinopharm Chemical Reagent Co. Ltd.), and  $\text{Yb}_2\text{O}_3$  (99.9%, Sinopharm Chemical Reagent Co. Ltd.) were thoroughly mixed in alcohol. The homogeneous mixture was then

calcined at 700–800 °C for 4 h in a muffle furnace. Then, 10 wt% polyvinyl alcohol (PVA) binder was uniformly added into the reground powders which were pressed into disk-shaped pellets of 10 mm in diameter and 2 mm in thickness. Finally, samples were sintered at temperatures of 1000–1300 °C for 4 h in an alumina crucible in air. The influence of rare earth ions co-doping concentrations on UCL performance in optimal UCL materials was studied. The optimal material was recorded as LC, the concentration of  $\text{Er}^{3+}$  ions was fixed at 1 mol%, and the molar ratio of  $\text{Er}^{3+}/\text{Yb}^{3+}$  ions was 1:1, 1:5, 1:10, 1:15, and 1:20.

The sintered ceramic samples were ground into powder and tested by an X-ray diffractometer (XRD, D/MAX 2550, Rigaku, Japan) with  $\text{CuK}\alpha 1$  radiation ( $\lambda = 0.154056$  nm) for phase structure analysis. The tube voltage is 40 kV, and tube current is 40 mA. The scanning speed is  $5^\circ/\text{min}$  in  $2\theta$  angle ranging from  $10^\circ$  to  $70^\circ$  at room temperature. The microstructure of the samples was analyzed by field emission scanning electron microscopy (SEM, S-4700, Japan). The UCL spectra of samples were recorded using a fluorescence spectrophotometer (F-7000, Hitachi High-Technologies Corporation, Tokyo, Japan), which was connected to a 980 nm laser by an optical fiber to provide a pumping light source. For temperature sensing measurement, the sample was placed on a hot platform controlled by a temperature controller (TP94, Linkam Scientific Instruments Ltd., Surrey, UK) with a heating rate of 10 K/min. The sample thickness was fixed to ensure the measurement accuracy.

### 3 Results and discussion

#### 3.1 Phase identification and microstructure

The powder X-ray diffraction patterns of  $x\text{La}_2(\text{WO}_4)_3-(1-x)\text{CaWO}_4$ : 1% $\text{Er}^{3+}$ , 5% $\text{Yb}^{3+}$  ( $x = 0, 0.2, 0.4, 0.6, 0.8, 1$ ) are shown in Fig. 1a. As  $x$  goes from 0 to 1, these diffraction peaks can be well indexed to the standard JCPDS 41-1431, 52-1718, and 15-0438 [24]. Accordingly, the crystal phase of  $x\text{La}_2(\text{WO}_4)_3-(1-x)\text{CaWO}_4$  co-doped with a small amount of rare earth ions (1 mol%  $\text{Er}^{3+}$  and 5 mol%  $\text{Yb}^{3+}$ ) transforms from pure  $\text{CaWO}_4$  ( $x = 0$ , tetragonal phase) to two solid solutions ( $0 < x < 1$ ) and then to pure  $\text{La}_2(\text{WO}_4)_3$  ( $x = 1$ , monoclinic phase). It is worth

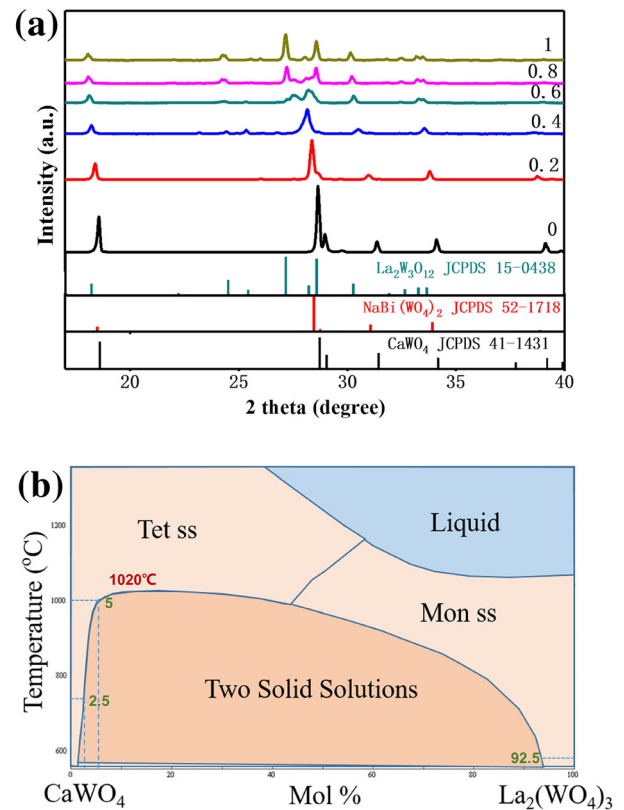


**Fig. 1** a XRD patterns of the as-prepared  $x\text{La}_2(\text{WO}_4)_3-(1-x)\text{CaWO}_4$ : 1% $\text{Er}^{3+}$ , 5% $\text{Yb}^{3+}$  ( $x = 0, 0.2, 0.4, 0.6, 0.8, 1$ ), and the standard pattern of PDF card JCPDS 41-1431, 52-1718, and 15-0438. b Binary phase diagram of  $\text{CaWO}_4$  and  $\text{La}_2(\text{WO}_4)_3$ . Tet ss and Mon ss refer to tetragonal scheelite and monoclinic scheelite, respectively [25]

mentioning that, when  $0 < x < 1$ , with the increase of  $x$ , the diffraction peak gradually moves to a smaller  $2\theta$  angles and widens ( $x = 0.2, 0.4$ ). The main crystalline phase of corresponding sample is isotypic with  $\text{A}^{(+1)}\text{B}^{(+3)}(\text{WO}_4)_2$ , belonging to tetragonal system structure. Then, the strongest peak gradually differentiated into two peaks ( $x = 0.6, 0.8$ ), which is consistent with the peaks of  $\text{La}_2(\text{WO}_4)_3$ . The above results can also be verified from the binary phase diagram  $\text{CaWO}_4$  and  $\text{La}_2(\text{WO}_4)_3$  in Fig. 1b [25]. The  $\text{CaWO}_4$ - $\text{La}_2(\text{WO}_4)_3$  compounds are discontinuous solid solutions, that is,  $\text{CaWO}_4$  and  $\text{La}_2(\text{WO}_4)_3$  phases can only dissolve into each other in a certain amount. According to the binary phase diagram, the maximum solubility of  $\text{La}_2(\text{WO}_4)_3$  in  $\text{CaWO}_4$  is 2.5 mol% at 740 °C and 5 mol% at 1000 °C, while that of  $\text{CaWO}_4$  in  $\text{La}_2(\text{WO}_4)_3$  is 7.5 mol% at 620 °C. At a temperature lower than 1020 °C, the above two phases give two-phase solid solution within the remaining

concentration range. This indicates that, when  $x$  is in the range of 0.2–0.8, both tetragonal and monoclinic phase exist in the  $x\text{La}_2(\text{WO}_4)_3-(1-x)\text{CaWO}_4$  materials.

The morphology of  $x\text{La}_2(\text{WO}_4)_3-(1-x)\text{CaWO}_4: 1\%\text{Er}^{3+}, 5\%\text{Yb}^{3+}$  ( $x = 0, 0.2, 0.4, 0.6, 0.8, 1$ ) is shown in Fig. 2. In pure  $\text{CaWO}_4$  ( $x = 0$ ), the internal grains are tightly bound together and almost no pores form. With the appearance and increase of  $\text{La}_2(\text{WO}_4)_3$  phase ( $x \geq 0.2$ ), the morphology of samples begins to change. When  $x = 0.4$ , columnar crystals are interleaved in the material, which helps to strengthen the material. Besides, from binary phase diagram of  $\text{CaWO}_4$  and  $\text{La}_2(\text{WO}_4)_3$ , the different composition ( $x$ ) of materials leads to a large change in the sintering temperature of materials. Therefore, finding suitable sintering temperature is conducive to good grain development.

### 3.2 Up-conversion luminescence property

The UCL spectra of  $x\text{La}_2(\text{WO}_4)_3-(1-x)\text{CaWO}_4: 1\%\text{Er}^{3+}, 5\%\text{Yb}^{3+}$  ( $x = 0, 0.2, 0.4, 0.6, 0.8, 1$ ) at room temperature, and the corresponding CIE chromaticity diagram are given in Fig. 3. It is clear that the UCL spectra of all samples consist of two green emission bands and a very weak red emission band. The two green emission bands have maxima at about 530 nm ( ${}^2\text{H}_{11/2} \rightarrow {}^4\text{I}_{15/2}$ ) and 552 nm ( ${}^4\text{S}_{3/2} \rightarrow {}^4\text{I}_{15/2}$ ),

respectively, while the weak red emission band is at 667 nm ( ${}^4\text{F}_{9/2} \rightarrow {}^4\text{I}_{15/2}$ ) [26, 27]. The luminescence intensity of all samples was normalized according to the intensity of  $\text{CaWO}_4: 1\%\text{Er}^{3+}, 5\%\text{Yb}^{3+}$ , as shown in the inset of Fig. 3a. With the increase of  $x$ , the UCL intensity of the strongest green emission band (552 nm) first increases and then gradually decreases, reaching the maximum at  $x = 0.2$ . As a result, the UCL intensity of the two-phase solid solution  $0.2\text{La}_2(\text{WO}_4)_3-0.8\text{CaWO}_4: 1\%\text{Er}^{3+}, 5\%\text{Yb}^{3+}$  is up to 33.5 times that of  $\text{CaWO}_4: 1\%\text{Er}^{3+}, 5\%\text{Yb}^{3+}$ . However, the enhancement ratio of the emission band, especially the red light at 667 nm, is not consistent with the green light at 552 nm. Therefore, in Fig. 3b, the UCL color of samples first obviously crosses to green region ( $x = 0.2-0.6$ ), and then moves towards yellow region ( $x = 0.8$  and 1). The  $x\text{La}_2(\text{WO}_4)_3-(1-x)\text{CaWO}_4: 1\%\text{Er}^{3+}, 5\%\text{Yb}^{3+}$  materials can emit a very high-purity green light and they will be competitive in these applications. According to the above UCL intensity and color purity,  $0.2\text{La}_2(\text{WO}_4)_3-0.8\text{CaWO}_4: 1\%\text{Er}^{3+}, 5\%\text{Yb}^{3+}$  was determined to be the optimal UCL material.

Furthermore, the effects of rare earth doping concentrations on the UCL performance were studied. The optimal UCL material has been determined to be  $0.2\text{La}_2(\text{WO}_4)_3-0.8\text{CaWO}_4: 1\%\text{Er}^{3+}, 5\%\text{Yb}^{3+}$ . It is well known that the doping concentration of rare earth ions has a very strong effect on the luminescence

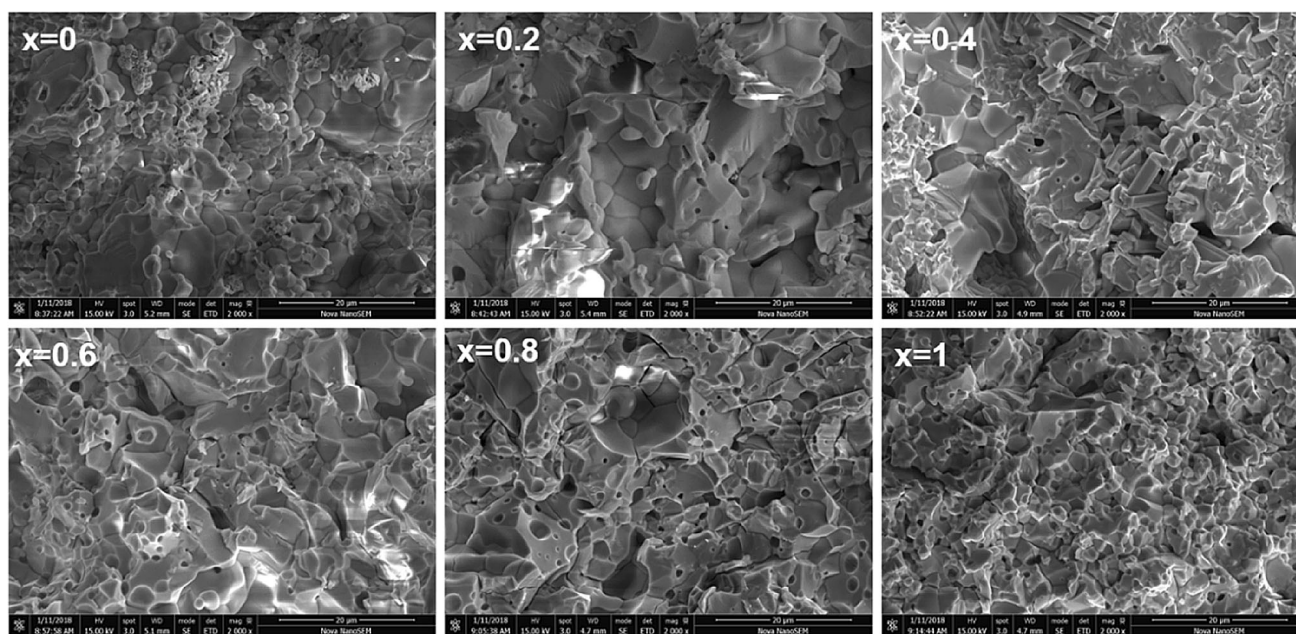


**Fig. 2** SEM images of  $x\text{La}_2(\text{WO}_4)_3-(1-x)\text{CaWO}_4: 1\%\text{Er}^{3+}, 5\%\text{Yb}^{3+}$  ( $x = 0, 0.2, 0.4, 0.6, 0.8, 1$ )



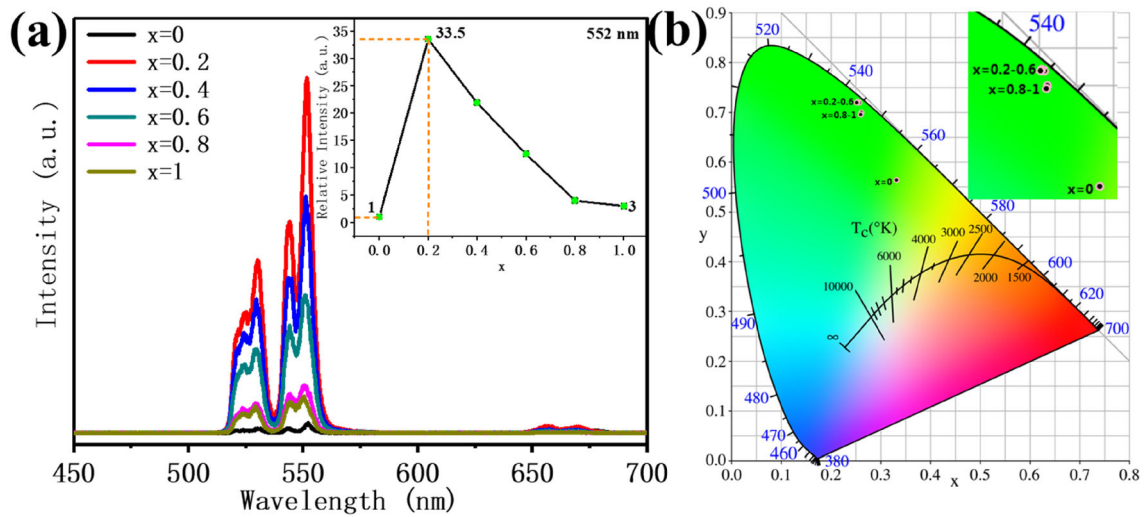


**Fig. 3** **a** The UCL spectra (the inset shows the  $x$  dependence of strongest peak) and **b** CIE chromaticity diagram of UC emissions for  $x\text{La}_2(\text{WO}_4)_3-(1-x)\text{CaWO}_4: 1\%\text{Er}^{3+}, 5\%\text{Yb}^{3+}$  ( $x = 0, 0.2, 0.4, 0.6, 0.8, 1$ ) under 980 nm laser excitation

intensity. For this reason, we studied the UCL spectra of  $\text{Er}^{3+}/\text{Yb}^{3+}$  co-doped  $0.2\text{La}_2(\text{WO}_4)_3-0.8\text{CaWO}_4$  materials with different  $\text{Yb}^{3+}$  co-doping concentrations, and the results are shown in Fig. 4a. The composition of UCL spectra of samples remains consistent with that in Fig. 3, which is composed of two strong green emission bands and a very weak red emission band. As  $\text{Yb}^{3+}$  concentration increases, the intensity of the strongest green emission band (552 nm) increases first and then gradually decreases, reaching the maximum value at the concentration ratio  $\text{Er}^{3+}/\text{Yb}^{3+}$  equal to 1:5. However, for the weak green emission and red emission, the intensity of

$\text{Er}^{3+}/\text{Yb}^{3+}$  at the concentration ratio of 1:5 and 1:10 does not differ significantly. This phenomenon can be explained by concentration quenching effect. With the increase of rare earth ions concentration, the distance between the adjacent rare earth ions becomes smaller, the interaction between the ions is enhanced, and the emission intensity of green light is weakened by partial non-radiative energy transfer. The quenching concentration of rare earth ions in different host is not constant, and some of them are relatively high, which may be caused by the entry of rare earth ions into the host lattice [28]. In addition, from the corresponding CIE chromaticity diagram of

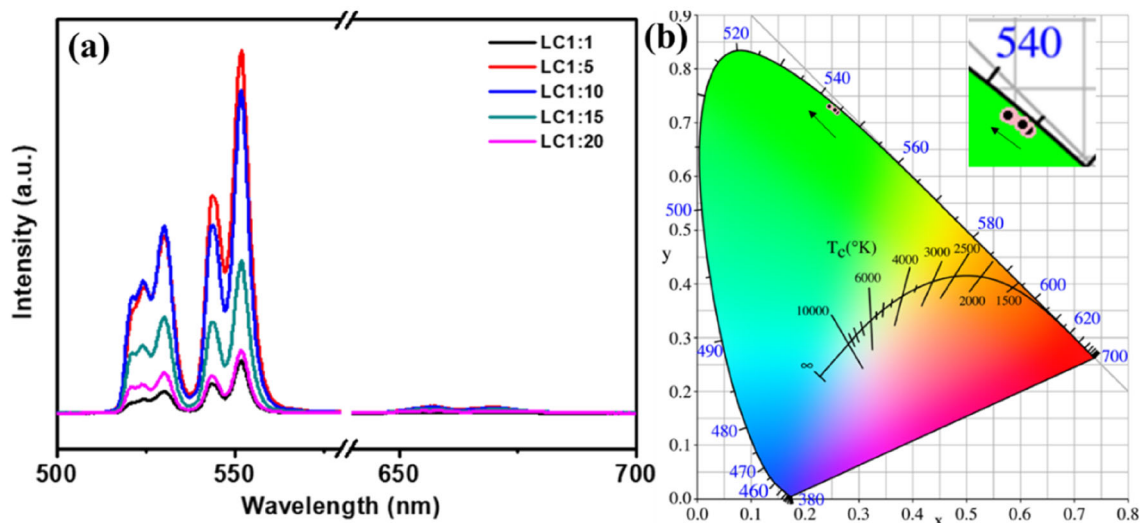


**Fig. 4** **a** The UCL spectra and **b** the corresponding CIE chromaticity diagram of  $0.2\text{La}_2(\text{WO}_4)_3-0.8\text{CaWO}_4: \text{Er}^{3+}, \text{Yb}^{3+}$

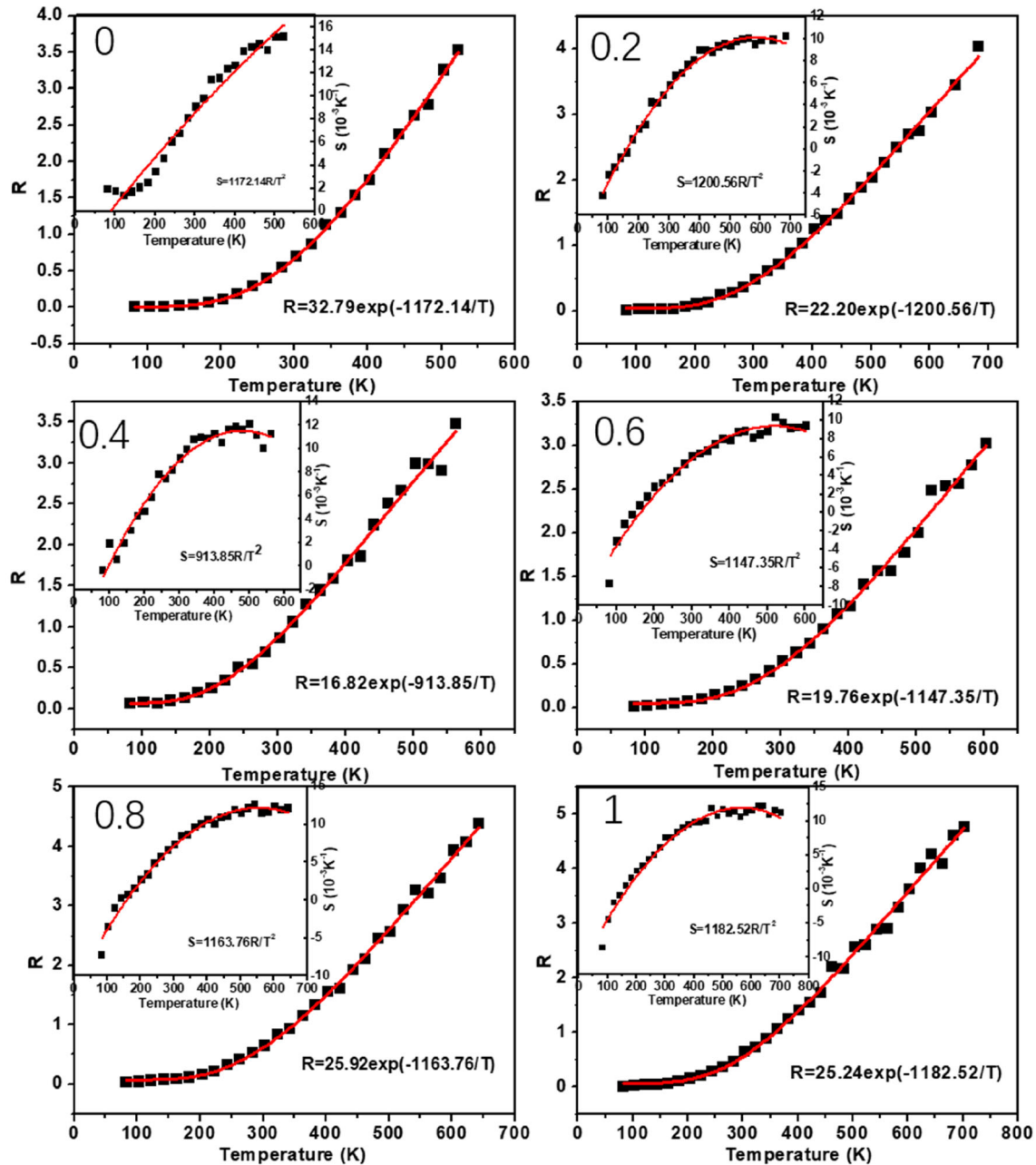


**Fig. 5** Temperature sensing properties of  $x\text{La}_2(\text{WO}_4)_3-(1-x)\text{CaWO}_4: 1\%\text{Er}^{3+}, 5\%\text{Yb}^{3+}$  ( $x = 0, 0.2, 0.4, 0.6, 0.8, 1$ ), namely, the temperature dependence of FIR and  $S$  (the inset)

$0.2\text{La}_2(\text{WO}_4)_3-0.8\text{CaWO}_4: \text{Er}^{3+}, \text{Yb}^{3+}$  given in Fig. 4b, it can be seen that with the increase of  $\text{Er}^{3+}/\text{Yb}^{3+}$  ion concentration ratio, the color gradually shifts to green region.

### 3.3 Optical temperature sensing property

Rare earth ion  $\text{Er}^{3+}$  has abundant energy levels, among which  ${}^2\text{H}_{11/2}$  and  ${}^4\text{S}_{3/2}$  are a pair of thermally

coupled energy levels. The transition of these two levels to the ground state level  ${}^4\text{I}_{15/2}$  produces two green emission peaks at 530 nm and 552 nm, both of which have a certain dependence on temperature. Therefore, the FIR technique can be used to measure temperature by the fluorescence radiated from the thermal coupling levels. The FIR and  $S$  can be expressed by the following formula [7, 29, 30]:  $\text{FIR} = \frac{I_{530}}{I_{552}} = Ae^{-\frac{\Delta E}{kT}}$ ,  $S = \frac{d\text{FIR}}{dT} = \text{FIR} \frac{\Delta E}{kT^2}$ , where  $A$ ,  $\Delta E$ ,  $k$ ,

**Table 1** The optical temperature sensing properties of  $x\text{La}_2(\text{WO}_4)_3-(1-x)\text{CaWO}_4: 1\%\text{Er}^{3+}, 5\%\text{Yb}^{3+}$  ( $x = 0, 0.2, 0.4, 0.6, 0.8, 1$ )

$x$	Temperature range (K)	$S_{\text{max}}/10^{-3} \text{ K}^{-1}$	$T_{S_{\text{max}}} \text{ (K)}$
0	83–523	15.14	523
0.2	83–683	10.26	683
0.4	83–563	12.07	503
0.6	83–603	10.24	523
0.8	83–643	12.58	543
1	83–703	12.2	623

$T$  is the constant, the energy separation between the two thermally coupled levels ( ${}^2\text{H}_{11/2}$  and  ${}^4\text{S}_{3/2}$ ), Boltzmann constant and absolute temperature, respectively. In Fig. 5, the fitting curve is shown for the temperature sensing properties (FIR and  $S$ ) of  $x\text{La}_2(\text{WO}_4)_3-(1-x)\text{CaWO}_4: 1\%\text{Er}^{3+}, 5\%\text{Yb}^{3+}$  ( $x = 0, 0.2, 0.4, 0.6, 0.8, 1$ ). With the increase of temperature, the FIR values measured in different temperature ranges all show a monotonically increasing trend. However, for sensitivity, the variation trend of  $S$  values with temperature varies from sample to sample. The fitted temperature sensing property data are listed in Table 1. Combined with Fig. 5, it is found that  $\text{CaWO}_4: 1\%\text{Er}^{3+}, 5\%\text{Yb}^{3+}$  shows a high temperature sensitivity  $S$  ( $0.01514 \text{ K}^{-1}$ ), but in a narrow temperature range of 83–523 K. Besides, from Fig. 3, the UCL intensity of both  $\text{CaWO}_4: 1\%\text{Er}^{3+}, 5\%\text{Yb}^{3+}$  and  $\text{La}_2(\text{WO}_4)_3: 1\%\text{Er}^{3+}, 5\%\text{Yb}^{3+}$  are lower than that of other UCL materials in this study. Some studies have shown that, in the process of variable temperature on UCL test, with the temperature increase, the intensity of green emission peak reduced gradually. The high power of 980 nm laser can have heating effect on the UCL material and affect the UCL property of materials. This means that, if low laser power is maintained, the optical signal-to-noise ratio of  $\text{CaWO}_4: 1\%\text{Er}^{3+}, 5\%\text{Yb}^{3+}$  and  $\text{La}_2(\text{WO}_4)_3: 1\%\text{Er}^{3+}, 5\%\text{Yb}^{3+}$  UCL materials will be very low, and the reliability of the measured data will be greatly reduced. Therefore, the performance of optical temperature sensing should be carried out on the premise that the luminescence intensity of materials is high enough with the increase of temperature under the excitation of low power laser. Obviously, the luminescence intensity of UCL materials with two-phase solid solution as host is significantly improved, among which the luminescence intensity of

$0.2\text{La}_2(\text{WO}_4)_3-0.8\text{CaWO}_4: 1\%\text{Er}^{3+}, 5\%\text{Yb}^{3+}$  increased the most significantly, which is far more than that of  $\text{CaWO}_4: 1\%\text{Er}^{3+}, 5\%\text{Yb}^{3+}$  and  $\text{La}_2(\text{WO}_4)_3: 1\%\text{Er}^{3+}, 5\%\text{Yb}^{3+}$  UCL materials. Moreover, in a wide temperature range, the two-phase solid solution UCL materials still maintain a high temperature sensing performance, as shown in Table 1.

## 4 Conclusions

In this study, in order to improve the UCL intensity and optical temperature sensing performance of tungstates, we adopted the approach of synthesizing two-phase material by regulating the relative content of cations  $\text{Ca}^{2+}$  and  $\text{La}^{3+}$  in  $\text{CaWO}_4\text{-La}_2(\text{WO}_4)_3$ . As a result, the UCL intensity has been greatly enhanced and the temperature sensing performance has been effectively improved. Specifically, when  $\text{Ca}^{4+}$  ion is gradually replaced by  $\text{La}^{4+}$  ion, XRD analysis shows that the crystal phase of the sample gradually changes from pure  $\text{CaWO}_4$  phase (tetragonal scheelite) to two-phase solid solutions of  $\text{CaWO}_4\text{-La}_2(\text{WO}_4)_3$ , and finally to the pure  $\text{La}_2(\text{WO}_4)_3$  phase (monoclinic scheelite). This trend can also be verified in binary phase diagram of  $\text{CaWO}_4$  and  $\text{La}_2(\text{WO}_4)_3$ . Correspondingly, the UCL intensity of two-phase solid solutions at 552 nm is much higher than that of pure phase material, of which  $0.2\text{La}_2(\text{WO}_4)_3-0.8\text{CaWO}_4: 1\%\text{Er}^{3+}, 5\%\text{Yb}^{3+}$  has the highest UCL intensity of 33.5 times of that of  $\text{CaWO}_4: 1\%\text{Er}^{3+}, 5\%\text{Yb}^{3+}$  materials. Further study on the influence of rare earth co-doping concentrations on UCL performance of  $0.2\text{La}_2(\text{WO}_4)_3-0.8\text{CaWO}_4: \text{Er}^{3+}, \text{Yb}^{3+}$  shows that the position of the emission peaks does not change, and the luminescence intensity coincidentally reaches the maximum at the  $\text{Er}^{3+}/\text{Yb}^{3+}$  ratio 1:5. Meanwhile, the temperature sensing performance of different hosts was studied, and the high temperature sensing sensitivity ( $0.01026 \text{ K}^{-1}$ ) was achieved in a wider temperature range of 83–683 K in optimal UCL material  $0.2\text{La}_2(\text{WO}_4)_3-0.8\text{CaWO}_4: 1\%\text{Er}^{3+}, 5\%\text{Yb}^{3+}$ . This research reveals that regulating cations content of host is a promising method to improve the UCL and temperature sensing performance.

## Acknowledgements

This work was supported by the China Postdoctoral Science Foundation (2019M651621).

## References

- P. Zhou, X.L. Yang, X.G. Wang, B. Hu, L. Zhang, W. Zhang, H.R. Si, Y. Zhu, B. Li, C.L. Huang, H.D. Chen, J. Chen, Y. Luo, H. Guo, R.D. Jiang, M.Q. Liu, Y. Chen, X.R. Shen, X. Wang, X.S. Zheng, K. Zhao, Q.J. Chen, F. Deng, L.L. Liu, B. Yan, F.X. Zhan, Y.Y. Wang, G.F. Xiao, Z.L. Shi, *Nature* **579**, 270 (2020)
- C.L. Huang, Y.M. Wang, X.W. Li, L.L. Ren, J.P. Zhao, Y. Hu, L. Zhang, G.H. Fan, J.Y. Xu, X.Y. Gu, Z.S. Cheng, T. Yu, J.A. Xia, Y. Wei, W.J. Wu, X.L. Xie, W. Yin, H. Li, M. Liu, Y. Xiao, H. Gao, L. Guo, J.G. Xie, G.F. Wang, R.M. Jiang, Z.C. Gao, Q. Jin, J.W. Wang, B. Cao, *Lancet* **395**, 497–506 (2020)
- M. De Curtis, F. Calzolari, A. Marclano, V. Cardilli, G. Barba, *Arch. Dis. Child. Fetal Neonatal Ed.* **93**, F55–F57 (2008)
- Y. Zhao, X. Wang, Y. Zhang, Y. Li, X. Yao, *J. Alloys Compd.* **817**, 152691 (2020)
- B. Dong, B.S. Cao, Y.Y. He, Z. Liu, Z.P. Li, Z.Q. Feng, *Adv. Mater.* **24**, 1987–1993 (2012)
- X.D. Wang, O.S. Wolfbeis, R.J. Meier, *Chem. Soc. Rev.* **42**, 7834–7869 (2013)
- Y. Zhang, X.N. Chai, J. Li, X.S. Wang, Y.X. Li, X. Yao, *J. Alloys Compd.* **735**, 473–479 (2018)
- X.Y. Li, X.T. Wei, Y.G. Qin, Y.H. Chen, C.K. Duan, M. Yin, *J. Alloys Compd.* **657**, 353–357 (2016)
- D.Q. Chen, M. Xu, S. Liu, X.Y. Li, *Sens. Actuators B* **246**, 756–760 (2017)
- X.F. Wang, Q. Liu, Y.Y. Bu, C.S. Liu, T. Liu, X.H. Yan, *Rsc Adv.* **5**, 86219–86236 (2015)
- W. Xu, Y. Cui, Y. Hu, L. Zheng, Z. Zhang, W. Cao, *J. Alloys Compd.* **726**, 547–555 (2017)
- M.C. Jia, G.F. Liu, Z. Sun, Z.L. Fu, W.G. Xu, *Inorg. Chem.* **57**, 1213–1219 (2018)
- K. Green, K. Huang, H. Pan, G. Han, S.F. Lim, *Front. Chem.* **6** (2018).
- R.S. Lei, X.Y. Luo, Z.Y. Yuan, H.P. Wang, F.F. Huang, D.G. Deng, S.Q. Xu, *J. Lumin.* **205**, 440–445 (2019)
- A. Pandey, V.K. Rai, *Dalton Trans.* **42**, 11005–11011 (2013)
- W. Xu, Y.W. Hu, L.J. Zheng, Z.G. Zhang, W.W. Cao, H.L. Liu, X.J. Wu, *J. Lumin.* **208**, 415–423 (2019)
- W. Xu, X. Gao, L. Zheng, Z. Zhang, W. Cao, *Sens. Actuators B* **173**, 250–253 (2012)
- Y. Zhang, J. Li, X.N. Chai, X.S. Wang, Y.X. Li, X. Yao, *J. Appl. Phys.* **121** (2017).
- Y. Zhang, X. Wang, Y. Li, Y. Li, X. Yao, *Opt. Mater. Express* **8**, 12–23 (2018)
- Y. Zhang, X.S. Wang, H.H. Ye, X. Gong, Y.X. Li, X. Yao, *J. Mater. Sci.* **29**, 19840–19845 (2018)
- W. Xu, X. Gao, L. Zheng, P. Wang, Z. Zhang, W. Cao, *Appl. Phys. Express* **5**, 2201 (2012)
- L. Li, L. Zheng, W. Xu, Z. Liang, Y. Zhou, Z. Zhang, W. Cao, *Opt. Lett.* **41**, 1458–1461 (2016)
- W. Xu, H. Zhao, Y. Li, L. Zheng, Z. Zhang, W. Cao, *Sens. Actuators B* **188**, 1096–1100 (2013)
- R.M. Hazen, L.W. Finger, J.W.E. Mariathasan, *J. Phys. Chem. Solids* **46**, 253–263 (1985)
- L.L.Y. Chang, *J. Inorg. Nucl. Chem.* **31**, 2003–2014 (1969)
- X. Chai, J. Li, X. Wang, Y. Li, X. Yao, *Opt. Express* **24**, 22438 (2016)
- J. Li, X. Chai, X. Wang, C.N. Xu, Y. Gu, H. Zhao, X. Yao, *Dalton Trans.* **45**, 11733–11741 (2016)
- X. Chai, J. Li, Y. Zhang, X. Wang, Y. Li, X. Yao, *RSC Adv.* **6**, 64072–64078 (2016)
- J.S. Zhong, D.Q. Chen, Y.Z. Peng, Y.D. Lu, X. Chen, X.Y. Li, Z.G. Ji, *J. Alloys Compd.* **763**, 34–48 (2018)
- X.J. Zhu, J.C. Li, X.C. Qiu, Y. Liu, W. Feng, F.Y. Li, *Nat. Commun.* **9** (2018).

**Publisher's Note** Springer Nature remains neutral with regard to jurisdictional claims in published maps and institutional affiliations.